DOE/DP/40200--113
DE90 006806

Effect of Barrier Layers in Burn-Through Experiments with 351-nm Laser Illumination

J. Delettrez, D. K. Bradley, P. A. Jaanimagi, and C. P. Verdon

Lab Report No. 208
February 1990

DISCLAIMER

Effect of Barrier Layers in Burn-through Experiments with 351-nm Laser Illumination

J. Delettrez, D. K. Bradley, P. A. Jaanimagi, and C. P. Verdon

Laboratory for Laser Energetics, University of Rochester, 250 East River Road, Rochester, New York 14623-1299

The time-resolved x-ray emission is measured from spherical targets consisting of glass shells overcoated with plastic in which thin signature layers are embedded. These targets are illuminated at 351 nm by the 24-beam OMEGA laser system at the Laboratory for Laser Energetics of the University of Rochester. We measure a large burn-through rate for bare plastic targets, which can only be replicated in 1-D hydrodynamic simulations with laser intensities in excess of ten times the nominal intensity. We observe that the burn-through times are affected by the presence of a thin outer coating (barrier layer). The burn-through times depend strongly on the barrier-layer material and thickness, whereas one-dimensional simulation results predict only a small effect. Several processes are considered to explain these results: illumination nonuniformity, early shine-through of the laser light through the plastic, prepulses, filamentation, self-focussing of hot spots, and the Rayleigh-Taylor instability. We conclude that mixing due to the Rayleigh-Taylor instability, enhanced by early shine-through, is the most probable cause of the observed large burn-through rates.

I. INTRODUCTION

In direct-drive inertial-confinement fusion (ICF), advanced target designs[1] require low-Z ablators ($Z < 6$), such as plastic, in order to minimize the radiative preheat of the fuel. It is therefore of importance to study the interaction of laser light with low-Z materials. One major area of study has been the measurement of the time-resolved mass-ablation rate in parylene [or polyparaxylylene, $(CH)_x$] by means of burn-through experiments (see Ref. 2 and references therein). In these experiments, the laser irradiates a spherical target that consists of a glass shell or a solid glass sphere overcoated with a parylene layer, in which one or more thin signature layers of moderate- to high- Z material have been embedded for diagnostic purposes to signal the penetration of the heat front. The onset time of the characteristic x-ray emission lines from a signature layer, which determines the mass-ablation rate, is compared to the onset time obtained from hydrodynamic code simulations. In transport experiments previously carried out on the OMEGA laser system at the Laboratory for Laser Energetics (LLE), the burn-through time through a layer of $(CH)_x$ overcoating a solid glass sphere occurred earlier than predicted by one-dimensional code simulations.[2] These burn-through times were successfully modeled by assuming that a small fraction of the laser energy (< 10%) was present in the laser-intensity distribution on target at two to three times the nominal laser irradiance (I_0), defined as the laser power divided by the target surface area. It was conjectured that small hot spots (< 20 μm in diameter) were responsible for the large burn-through rates. This conclusion was supported by subsequent measurement and modeling of the laser far-field pattern which showed that such hot spots could be produced by small phase errors present in the beam before focusing .[3]

While it was concluded in Ref. 2 that laser illumination nonuniformity (mainly caused by hot spots) was the probable cause of departure from predicted behavior, other processes have been suggested to explain the results. These processes can be divided into two types: laser interaction processes and hydrodynamic instabilities. Laser interaction processes include, in addition to laser irradiation nonuniformity, shine-through of the laser light early in the pulse while the parylene is still transparent, prepulses, filamentation, and self-focusing of the hot-spots. Shine-through and prepulses lower the effective areal density of the parylene while filamentation and self-focusing produce regions of intensity higher than nominal. The main hydrodynamic instability is the Rayleigh-Taylor instability, which can be "seeded" by target imperfections and laser interaction processes. There are two unstable regions, the ablation surface and the $(CH)_x$–signature-layer interface. The evolution of the Rayleigh-Taylor instability in either of these regions could result in mixing, which would bring signature-layer material closer to the heat front and produce an early burn-through signal.

In this paper, we report on two series of burn-through experiments on imploding spherical shell targets undertaken to study to what extent the various processes discussed above contribute to the measured enhanced burn-through rate. In particular, we had observed in implosion experiments that slower burn-through rates resulted from the addition of a thin barrier layer of Al (<0.1 μm) on the outside of the target. In the first series of experiments, we studied the effect of adding an Al barrier layer; in the second series, we studied the effect of varying the material and the thickness of the barrier layer. We show that the laser interaction processes cannot produce the observed burn-through times. We conclude that mixing due to the Rayleigh-Taylor instability is a possible explanation of the enhanced burn-through rate observed in these two series of experiments.

II. DETAILS OF THE EXPERIMENT AND SIMULATIONS

The first series of experiments was carried out to study the effect of adding an Al barrier layer and of varying the thickness of the parylene layer on the burn-through rate. The targets consisted of 3-μm thick glass shells, with diameters ranging from 300 to 400 μm, coated with a layer of $(CH)_x$ with thickness varying from 0 to 9 μm (some of the targets contained more than one layer of parylene separated by 0.1-μm layers of either Mg or Al). Several targets were overcoated with a 0.1-μm thick barrier layer of Al. The targets were irradiated by the OMEGA laser system at 351 nm with 600-ps FWHM Gaussian pulses at intensities ranging from 6×10^{14} to 1×10^{15} W/cm^2. The beams were focused tangentially to the targets to optimize overall uniformity and absorption. The burn-through time was defined as the onset of the signature layer emission (H- and He- like resonant lines) as measured with SPEAXS.[4] SPEAXS is a time-resolving spectrometer in which an elliptically curved PET (Pentaerythritol) crystal analyzer disperses the x-ray spectrum (1.5–2.5-keV range) onto the slit of an x-ray streak camera. An absolute timing reference to the incident laser pulse was provided by a separate 264-nm fiducial signal generated by quadrupling a small fraction of the OMEGA 1.054-μm pulse.[5] The simulations were carried out with the 1-D hydrodynamic code LILAC,[6] in which the ionization levels and the radiation opacities and emissivities for the signature and barrier layer materials were calculated from a non-LTE (local-thermodynamic-equilibrium), average-ion formulation. The value of the flux-limiter was taken as f=0.06 (sharp cut-off method). This value for the flux-limiter is routinely used in all target simulations at LLE as it gives the best agreement with measured laser absorption fractions and implosion velocities over a large range of experimental conditions, including the present ones (see for example the results of simulations of high-density experiments in Ref. 7).

The results of these experiments are displayed in Fig. 1, in which the burn-through time is plotted against the ablated areal density of the parylene obtained from targets with increasing thicknesses of parylene. (The value of the ablated areal density is almost equal to that of the thickness of the parylene layer in centimeters since the density of parylene is 1.1 g/cm^3.) For a given parylene thickness (or ablated areal density) the burn-through time is earlier for the bare parylene targets (triangles) than for the Al-coated targets (squares). The rate of ablation of the parylene (the inverse of the slope of a curve drawn through the points) is larger for the targets without an Al barrier layer. The dashed lines, which are the results of simulations at laser intensities bracketing the range of experimental intensities, have a slightly slower ablation rate than for the targets with the Al barrier layers. Actual case-by-case simulations required laser intensities of about ten times the nominal intensity to match the burn-through times of the bare parylene targets and about three times the nominal intensity for the Al-coated ones. It should be noted that the burn-through rates measured for the bare parylene targets are larger than those measured in Ref. 2, in which the targets were also bare. This difference may be attributed to changes in the OMEGA system driver between the two experiments.

It is difficult to attribute the large burn-through rates for the bare parylene targets solely to hot spots with intensity larger than ten times the nominal intensity. This would require the presence of hot spots with intensities larger than twenty times nominal in individual laser beams because the intensity of single-beam hot spots relative to nominal intensity is reduced by about a factor of two from the overlap of the 24 beams of OMEGA.[8] In Ref. 2, the value of the intensity required to simulate the measured burn-through time was interpreted as a measure of the intensity of the hot spots in the laser illumination. In light of the present results, this intensity should now be interpreted as an indication of the

strength of the processes that cause the early onset of x-ray emission from the signature layer.

The second series of experiments was conducted in order to investigate two main issues: whether a non-opaque barrier layer would also reduce the burn-through rate and whether materials with a higher Z than Al would be more effective as barrier layers. To that end, targets with parylene layers of the same thickness were overcoated with barrier layers of varying materials and thicknesses. Of particular interest were transparent materials with a nuclear charge Z larger than that of $(CH)_x$, such as KCl. The targets consisted of 3-μm thick glass shells covered with a signature layer of 0.1-μm thick Al (except for the bare target and Al barrier layer target which had a Au signature layer), a 6-μm thick layer of $(CH)_x$, and a barrier layer with the materials and thicknesses listed in Table I. These targets were irradiated by the OMEGA laser system at 351 nm with 600-ps FWHM pulses at an intensity of of $8\pm1 \times 10^{14}$ W/cm^2. The beams were focused tangentially to the targets and the burn-through time was measured with SPEAXS as described previously.

The temporal profiles of the Al H-α line emission or of the Au M-band emission near 2 keV (the continuum from the $(CH)_x$ was subtracted) are shown superimposed in Fig. 2. The burn-through times with respect to the peak of the laser pulse, defined as the time at which the signature emission reaches ten percent of the maximum value, are listed in Table I. The burn-through times for the bare target and for the Al-coated target (parylene areal density of about 6.7×10^{-4} g/cm^2) are about the same as those measured in the first series of experiments (Fig. 1). With the exception of the KCl barrier layer, the burn-through time increases as the average nuclear Z of the outer layer material increases from none (bare CH) to 79 . The KCl case is an exception because the burn-through time is 125 ps earlier than that for Al, even though KCl and Al have roughly the same average Z (18 and 13) and mass density (2.7 and 2.0 g/cm^3) . The fact that the laser intensity was slightly

lower for the Al barrier layer case is not sufficient to explain this difference (this point will be discussed with the simulation results in the next paragraph). Finally, increasing the thickness of the gold layer delays the onset of the burn-through signature, but by a larger amount than would be expected from the substantial increase in the barrier layer areal density. (This point will be discussed in more detail in the discussion section.) The burn-through is marginal for the 0.05–μm gold case, as can be seen from the weak emission from the signature layer, i.e., the heat front barely reached the signature layer.

Simulations were performed with the hydrodynamic code LILAC to determine whether the change in burn-through time with Z is due to the added mass of the barrier layer and to the energy lost to ionization and x-ray radiation in the high-Z layer. Each of the cases was first run at nominal intensity and then at progressively higher intensities until the burn-through time matched the measured time. The results are shown in Table I, along with the experimental conditions and results already discussed. There is no burn-through at nominal intensity for any of the cases and the burn-through is marginal (burn-through times greater than 300 ps after the peak of the pulse) at one and half times nominal intensity for most of the cases. The dependence of the burn-through time on the laser intensity normalized to the nominal intensity is shown in Fig. 3 for the following cases: bare, Al, and KCl. It nearly follows a curve of constant energy, i.e., the locus of times at which the integrals of Gaussian laser pulses with increasing peak power yield the same energy. The curves in Fig. 3 do not exactly follow the curve of constant energy because the absorption is larger at low intensity than at high intensity. Because the burn-through time is very sensitive to the laser intensity at low intensities, for the marginal burn-through cases a small change in the laser intensity can result in a large change in the burn-through time. For example, at twice nominal intensity in Table I, when the Al case was calculated with the

same laser intensity as the KCl case, the burn-through time, shown in parentheses, was 20 ps less than for the KCl case rather than 210 ps longer.

The burn-through time itself is not the best quantity for analyzing the results because comparison can only be made between cases with the same target conditions (especially the parylene thickness) and the same laser parameters (laser intensity and pulse width). A preferable quantity is the ratio I_m/I_0, where I_m is the laser intensity required in the simulations to match the measured burn-through times. This quantity is obtained from Fig. 3 by determining the intensity at which the measured burn-through time (the horizontal bands) matches the time from the simulation. The matching intensities I_m for all the cases are listed in Table I, where the uncertainties in I_m are obtained from the experimental uncertainty in the burn-through time (the width of the horizontal bands). The value of I_m decreases from its largest value, over 12 times nominal for the bare-parylene case, as the nuclear Z of the barrier layer increases and is only 1.5 nominal for the thick gold case. Again, the KCl barrier layer case is an exception to the trend.

DISCUSSION

The results of the LILAC simulations lead to three observations: 1) there is little difference in the effect of the Al, KCl, CsI, and 0.015-μm Au barrier layers, 2) the addition of these barrier layers should change the burn-through time by at most 50 ps, and 3) the 0.05-μm Au barrier layer has the most effect on the burn-through time, i.e., the simulation requires only 1.5 I_0 to obtain the experimental value. (No burn-through was observed at 1.25 I_0). This is in contrast to the experimental results where the burn-through time increases with the nuclear Z of the barrier material (except for the KCl case), where there is a large difference in burn-through time between the bare case and the aluminum-coated case, and where the burn-through rate for the KCl barrier layer case is much larger than that of the Al case. One source of agreement between the experimental and simulation results is

the fact that the onset of the signature layer for the thick gold barrier layer is delayed from that of the thin gold barrier layer. Even there, the difference in the onset time is smaller in the simulation than in the experiment.

In order to attempt to explain the results, we investigated with the code LILAC the possibility that the following processes, discussed in the introduction, could lead to enhanced burn-through rates:

- Hot spots of intensities exceeding ten times nominal.
- Shine-through of the laser light early in the pulse (or of a prepulse) while the parylene layer is still transparent.
- A prepulse that would ablate part of the bare parylene layer.
- Self-focussing of the hot spots and filamentation.
- Mixing caused by the Rayleigh-Taylor instability.

To appreciate how the barrier layers can affect these processes, the electron density profiles in the corona 300 ps before the peak of a nominal intensity pulse are displayed in Fig. 4 for four barrier layer cases: bare $(CH)_x$, 0.1 μm of Al, 0.015μm of Au, and 0.05 μm of Au. This particular time was chosen because it shows conditions in the corona just before the observed burn-through time for the bare $(CH)_x$ case. The electron density is plotted as a function of radius; the electron temperature in the corona is about 1 keV in all cases. The thicker part of the line shows where the barrier-layer material is present. The profile for the thick-gold case has been shifted to the left for clarity. Two observations should be noted in Fig. 4: The density profiles for all the cases except the thick-gold case are approximately the same; the Al and the thin-gold barriers layers have been ablated to densities below one-tenth the critical density.

The first process considered is the presence of hot spots, which can result in two effects: an enhanced penetration of the heat front (as discussed in Ref. 2) and hole-

drilling,[9] which, through lateral transport, brings laser-heated material in contact with colder surrounding material, including the signature layer material. One-dimensional simulations of burn-through experiments indicate that hole-drilling can lead to earlier burn-through than the enhanced penetration of the heat front. In this explanation the effect of the barrier layers would be the smoothing of the hot spots with x rays. There are three reasons why the presence of hot spots does not explain the observed burn-through rates. First, in order to explain the experiment results, the hot spots in individual beams would have to be about twenty times nominal because the superposition of the 24 beams of OMEGA smooths out the illumination pattern.[8] But time-integrated x-ray and equivalent-target-plane imaging do not show the presence of hot spots with such high intensities. Second, the barrier layers cannot be expected to smooth out the hot spots. By 300 ps before the peak of the pulse (see Fig. 4) the aluminum and thin gold barrier layers are already far into the blow-off, at densities below 0.01 critical density. Up to that time the x-ray radiation efficiency was limited by the low electron temperature. For times later than -300 ps, when the effect of the hot spots is more pronounced because of the increasing laser intensity, the barrier layer material is too far in the blow-off to be effective. The third reason is that the Z-dependence of the burn-through rates is not consistent with radiation smoothing: the KCl case has a larger burn-through rate than Al even though its average Z is larger. Finally, hole-drilling can also be ruled out as a possible process because the same arguments on radiation smoothing apply.

The second process considered, shine-through, assumes that, because $(CH)_x$ is transparent to u.v. light at room temperature, laser light would penetrate to the signature layer early in the pulse before breakdown. This process is very attractive because it would explain both the effect of adding a thin barrier layer of aluminum and the difference in burn-through time between the Al and KCl cases. (CsI is also transparent at room temperature,

but its use as a photocathode material implies that free electrons can be created very quickly by the laser pulse.) The aluminum layer is thick enough to block the laser light early in the pulse (its skin-depth for 0.351-μm light is 0.0120 μm), while KCl seems to behave partly like parylene and partly like an opaque conductor. An opaque barrier layer can prevent prepulses or the early part of the pulse from penetrating into the target and depositing energy inside the target where breakdown occurs. Breakdown thresholds for high-intensity laser illumination in parylene and glass are not well known.[10] In the targets used in this experiment, breakdown probably occurs at the parylene–signature-layer interface, especially when the signature layer is an opaque material which absorbs some of the laser light reaching it. This interface can also be the site for impurity deposition during the target coating process and for target imperfections.[11]

A simple model was developed in LILAC to study the effects of breakdown due to shine-through. The purpose of the model is not to describe exactly the complex breakdown process in the parylene, but to present a probable behavior of the parylene during the shine-through phase of the interaction. In the model, the parylene is assumed transparent to the laser light until breakdown occurs. At a given intensity threshold (10^{11} - 10^{12} W/cm^2), the breakdown at the interface is modeled by depositing all the laser energy into electrons at the boundary of the parylene and signature layers. The electron temperature increases in the region immediately in front of the deposition region because of thermal conduction. (The electron thermal conductivity used in the model is that of Spitzer[12] with a floor at 1 eV.) A critical surface is created in that region as the parylene ionizes or breaks down. Because it is difficult to model the breakdown and the ionization of parylene at solid density and temperatures below one electron volt, this critical surface cannot be created self-consistently. Instead, the laser light is deposited in the zone where the electron temperature reaches a few electron volts (varying this threshold temperature makes little difference).

This causes an "ionization wave" to propagate quickly (in about 50 ps) from the signature layer to the target surface. As the laser intensity increases in time, the critical surface reaches the outer surface of the target. (About one Joule has been deposited in the plastic by this time.) At that point, a cavity with density varying between one-third solid and almost three times solid density has formed in the slowly expanding parylene layer. An ablation surface is then established and the plastic layer is recompressed to conditions very near those obtained in the absence of shine-through. As a result, burn-through times are not affected by shine-through. However, a possible effect of shine-through is that a nonuniform energy deposition at the parylene–signature-layer interface may lead to a nonuniform low-density plasma in the parylene layer by the time the ablation surface is established. These conditions may seed the Rayleigh-Taylor instability during the recompression, which may lead to mixing of signature layer material into the parylene. This process will be discussed later.

The presence of a laser prepulse is also a possible explanation because the burn-through rates increased from that of Ref. 2 after changing the oscillator and removing the prepulse suppressor in the OMEGA laser system. A prepulse absorbed on or close to the surface of the target would have the effect of removing target material before the arrival of the main pulse. As such, the presence of a 0.1-μm Al barrier layer should not make any difference. Also, from Fig. 1 we estimate that about 4 μm of parylene would have to be ablated to bring the 8-μm burn-through time for the bare target in line with the time for the aluminum-coated target. Ablating 4 μm of plastic requires about 600 Joules of energy, which is far more than can be delivered by a prepulse. Prepulse measurements on the OMEGA laser have led to the conclusion that if a prepulse existed, its energy would be less than one millijoule. Therefore, the presence of a prepulse must be ruled out as a cause of the enhanced burn-through rate.

Filamentation and self-focussing could be responsible for the observed fast burn-through times because they can lead to local laser intensities larger than those applied to the target and, therefore, to higher estimates of the maximum intensity in the laser illumination. A distinction is made between the two processes: filamentation arises from initial small perturbations in the laser illumination, whereas self-focussing involves the entire beam or a hot spot treated as a beam. For the burn-through experiments, self-focussing of hot spots, rather than of the entire beam, is considered because the laser beams are focussed tangentially to the target. These processes are divided into two types, ponderomotive and thermal, depending whether the plasma is forced out of the high intensity region by the ponderomotive force of the laser light or by the high pressures resulting from high temperatures. Filamentation and self-focussing have no laser intensity thresholds for their onset. (There exists a critical laser power for ponderomotive self-focussing, but its value is orders of magnitude lower than the laser powers of interest.[13]) A requirement is that there should be enough plasma for the two processes to develop and for the light to focus to high intensities, i. e., their growth-lengths must be shorter than the plasma scale length. Also, self-focussing occurs only for initial hot-spot radii larger than the equilibrium radius for self-trapping,[13] which is of the order of a few vacuum wavelengths. Code results for simulations of thermal filamentation or self-focussing are not available for the experimental conditions that apply here: a sub-nanosecond laser pulse illuminating a solid plastic pellet and creating electron density scale lengths of the order of 50 μm. The only characterization available for filamentation and self-focussing is their growth-length scaling as obtained from simple models that assume uniform plasmas and usually neglect laser light absorption and heat conduction.

The growth-lengths for ponderomotive and thermal filamentation are given, respectively, as the axial wave number of the fastest growing mode:[14]

$$k_p = \frac{1}{8}\left(\frac{v_0}{v_{th}}\right)^2 \frac{\omega_{pe}^2}{k_0 c^2}$$

and

$$k_{th} = \frac{\omega_{pe}}{7.5 k_0 c} \frac{v_o}{v_{th}} \frac{1}{\lambda_{ei}}$$

where v_o is the quiver velocity, v_{th}, the thermal velocity, ω_{pe}, the plasma frequency, k_o, the laser wave number, and λ_{ei}, the electron-ion collision mean-free-path. It should be noted that the ponderomotive growth-length is independent of the Z of the material. At the time of the burn-through in the parylene the conditions are: T_e = 1 keV and I = 1 x 10^{14} W/cm^2. For these conditions and for the ratio of the critical density to the electron density n_c/n_e = 10, the ponderomotive growth-length is about 2 mm and the thermal growth-length, 1.6 mm. While estimates of these growth-lengths may vary (for example, another estimate[15] yields about 1.0 mm and 0.6 mm for the ponderomotive and thermal filamentation growth-lengths respectively), the growth-lengths exceed by about an order of magnitude or more the distance between the tenth-critical and the critical surfaces at burn-through time (see Fig. 5, for distances typical of the experiments discussed in this paper).

The growth-lengths for self-focussing are more difficult to obtain, but a rough estimate of the ponderomotive growth-length is available.[13] The inverse of the ponderomotive self-focussing distance is given by

$$R_p^{-1} = \frac{\omega_{pe}}{\sqrt{3}\, k_0 c} \frac{v_0}{v_{th}} \frac{1}{r_0} \left(1 - \frac{n_e}{n_c}\right)^{-\frac{1}{2}}$$

where r_0 is the beam or hot-spot radius. For the conditions described above, we get R_p = 3.5 r_0, or for a hot spot of 20 μm, R_p = 35 μm. It is therefore possible for hot spots with intensity two or three times nominal to self-focus and to produce intensities ten times nominal.

To compare the effectiveness of ponderomotive self-focussing in the presence of the various barrier layers, we compare the scale-lengths in the corona obtained from the simulations for each of the barrier layer cases (the ponderomotive self-focussing does not depend on the Z of the material). Fig. 4 shows that, 300 ps before the peak of the pulse, the scale-lengths for bare CH and for the aluminum and thin gold layers are almost the same. For the thick gold layer, the scale lengths are shorter than for the other layers because the quarter-critical surface has barely burnt through the gold layer. The distance between the critical surface and the one-tenth critical surface, where self-focussing is more likely to occur, is plotted as a function of time in Fig. 5. This distance is longer early in the pulse for the low-Z barrier layers, reflecting the steepening of the scale-length for higher Z materials. But, after the one-tenth critical surface has burnt through the barrier layer, the effect is reversed and the scale lengths are longer for the higher Z cases. This is caused by early radiation preheat which heats the cold $(CH)_x$ and increases the mass-ablation rate. Despite these differences, the distances between the two surfaces for $(CH)_x$, aluminum, and thin gold are the same within less than ten microns; only the thick gold case leads to much shorter distances. Thus, if self-focussing were occurring, it should be no different for the bare, aluminum, and thin gold cases; this is especially true since, as early as 300 ps

before the peak of the pulse, these layers have been ablated below one-tenth critical and should not affect self-focussing between that surface and the critical surface.

We now consider the Rayleigh-Taylor instability, which occurs when a light fluid is accelerated against a heavier fluid and which could cause the large observed burn-through rates by mixing signature-layer material into the parylene layer. The instability can occur in two regions of the target: at the ablation surface and at the signature–layer-parylene interface. Near the ablation surface, the cold dense shell material is accelerated by the hot, less-dense ablating material during the inward acceleration phase of the target motion. This situation is analogous to the classical Rayleigh-Taylor fluid instability[16] and is often referred to as the acceleration phase or ablation surface instability. Numerical simulations have shown, however, that the linear and non-linear growth rates for the ablation surface instability are different from those expected from the classical case because they are modified by the ablation process.[17-19] In the burn-through experiments the possible existence of unstable flow development is further complicated by the presence of the unstable interface located at the parylene–signature-layer boundary, where the lighter parylene is accelerated against the denser signature-layer material. The unstable evolution of this interface is expected to be nearly classical.

The Rayleigh-Taylor instability is analyzed by decomposing the fluid perturbation into Legendre modes. The evolution of the instability can then characterized by the growth rates of these modes. The growth rates are usually functions of wave numbers (k), which are related to the Legendre modes (ℓ) by $k^2 = \ell(\ell+1)/R_0^2$, where R_0 is the average radius of the perturbation. In the references cited above, the growth rates were calculated mostly for single modes. However, a number of recent experimental and theoretical studies[20,21] have shown that the contributions of all potentially unstable modes and their mode-mode interactions must be considered. The treatment of all of these modes,

including both their linear and their nonlinear evolution, during the pellet motion is presently beyond the capabilities of ICF simulation codes. However, models have been developed that estimate the unstable growth and the potential effect of the Rayleigh-Taylor instability on pellet implosions from the zeroth-order (unperturbed) hydrodynamic information obtained from one-dimensional simulations.[21] The evolution of the unstable growth is carried out in a postprocessor to LILAC and, thus, the effects of the instability are not fed back into the one-dimensional simulation.

A model similar to that described in Ref. 21 has been developed to estimate the amount of shell distortion and mixing that could take place during the inward motion of burn-through targets. This model computes the modal amplitudes due to the Rayleigh-Taylor unstable flow development and estimates from these amplitudes the mixing region depth, which is of the order of σ_{rms}, where σ_{rms} is given by[21]

$$\sigma_{rms} = \left[\frac{1}{4\pi} \sum_{\ell > 1} \sum_{m} | A_{lm} |^2 \right]^{\frac{1}{2}}$$

where A_{lm} are spherical harmonic modal coefficients. Starting from small perturbation seeds, the modal amplitudes grow exponentially, with growth rates that are different at the two unstable surfaces because the rates for the ablation surface instability are modified by the ablation process. (This phase of the development of the instability is called the linear growth phase and the rates are referred to as linear growth rates.) As the instability evolves into the non-linear phase, bubbles develop inward toward the high-density side of the ablation surface and spikes grow toward the outside of the target. The model tracks the growth of individual modes using the linear growth rates until some saturation amplitude is reached, at which point the amplitude rms is obtained from a phenomenological model.

Details of the treatment of saturation, which are too complex to review here, are found in Ref. 21.

We first consider the development of the ablation surface instability. For low-Z ablators, which have short-density scale lengths near the ablation surface, the linear growth rates can be expressed as[17,22] $\gamma = \alpha \sqrt{ka} - \beta k V_a$, where k is the unstable mode wave number, a, the acceleration , and V_a, the ablation velocity given by $\dot{m}/\hat{\rho}$ ($\dot{m}$ is the mass flux rate and $\hat{\rho}$, the peak density). The constant values $\alpha \approx 0.90$ and $\beta \approx 3\text{-}4$ provide an adequate fit to the growth rates obtained from full two-dimensional simulations over a wide range of initial parameters. The constant α is approximatly equal to $A^{1/2}$, where A is the Atwood number defined as $[(\rho_H - \rho_L) / (\rho_H + \rho_L)]$, where ρ_H is the density of the heavy fluid (the signature-layer material) and ρ_L is the density of the light fluid (parylene). Comparisons with growth rates determined by simulations with the two-dimensional hydrodynamic code ORCHID[23] for the experiments of interest showed that this expression with β=3 gives a good fit. For this case we are interested in the development of the bubble, which has the potential of reaching into the signature layer. Its amplitude is given by[21] $\sqrt{2}\sigma_{rms}$. After a given mode has reached saturation, the amplitude of the bubble is assumed to continue to grow linearly in time.[24] (Studies have shown that, for finite fluid layers in the non-linear phase, the motion of the bubble departs from constant velocity as the layer thickness gets small.[25] However, since this model is used only to illustrate the potential effects of the instability, no attempt has been made to treat the saturation stage more accurately.)

For the evolution of the parylene–signature-layer interface instability during the implosion the linear growth rates are given by $\gamma = \sqrt{Aka/(kL + 1)}$, where A is the Atwood number and L is the mass-density scale length . In this case we are interested in the evolution of the spike because we want to estimate to what extent the signature-layer

material can penetrate into the parylene layer toward the laser. During both the linear and non-linear growth phase, the amplitude of the spike is taken as $\sqrt{2}\,(1+A)\,\sigma_{rms}$.[21]

In order to obtain an estimate of the mixing layer depth in burn-through targets, we consider a range of simple initial amplitude cases. We assume that the laser illumination nonuniformity produces the dominant source of initial amplitude seeds to the Rayleigh-Taylor instability and can be represented[26] by $A_{lm}(t=0) = \xi_0 \exp\{-(\Delta R/R)\,\ell\}$ (μm/mode), where ℓ is the Legendre mode number . (The modes are assumed to be symmetric in the azimuthal direction.) For the purpose of this paper, the constant $\Delta R/R$ controls the mode spectrum of the initial seed amplitude. For the first case we consider $\Delta R/R = 0.05$ and three values of ξ_0 such that $\sigma_{rms1} = 0.304$ μm, $\sigma_{rms2} = 0.167$ μm, and $\sigma_{rms3} = 0.0304$ μm, where σ_{rms} is defined as before. For the second case we set $\Delta R/R = 0.01$ and adjust ξ_0 such that the same values of σ_{rms} are obtained. The spectral distribution for the two values of $\Delta R/R$ are shown in Fig. 6. The two values were chosen to emphasize different regions of the spectrum: the case in which $\Delta R/R=0.05$ contains mostly lower-order modes whereas the other case, $\Delta R/R=0.01$, has a flat mode spectrum. The targets are 3-μm glass shells coated with parylene thicknesses varying from 4 μm to 10 μm and with radii and incident laser intensity similar to those in the experiments described in this paper. Fig. 7 displays an example of the model prediction for the thickness of the mix layers that could potentially be generated by the growth of the Rayleigh-Taylor instability as a function of time for two cases: a 4-μm parylene layer (Fig. 7a) and a 6-μm parylene layer (Fig. 7b). The initial conditions for both cases are $\sigma_{rms} = 0.167$ μm and $\Delta R/R = 0.05$ μm. The solid line is the in-flight thickness of the parylene, defined as the difference between the position of the overdense portion of the target and the position of the parylene-glass interface. The position of the overdense portion of the target is determined by searching for the location of the peak in the density from the outer radius inward and determining the radial location of the e-fold

from the peak density outward. The dashed lines show the increase with time of the thicknesses of the unstable regions associated with the ablation surface (A) and with the parylene-glass interface (I). For the initial conditions used in this example the ablation surface instability has the largest mixing region. No mode coupling was assumed between the ablation surface and the parylene-glass interface in order to illustrate the respective evolution of the two unstable regions. (If a coupling of the form exp(-k Δr) were assumed,[16] where Δr is the distance between the two surfaces, larger growth would be obtained at the parylene-glass interface.)

The signature times, defined as the time of the earliest cross-over of either of the dashed curves with the parylene thickness curve, are shown in Fig. 8 for parylene thicknesses of 4 to 10 μm . The curves labeled 1, 2, and 3 represent the signature times for the cases with initial amplitude of 0.304 μm, 0.167 μm, and 0.0304 μm, respectively. Fig. 8a is for $\Delta R/R = 0.05$ and Fig. 8b, for $\Delta R/R = 0.01$. The resulting signature times show that, depending on the modal spectrum and amplitudes, the Rayleigh-Taylor instability could grow fast enough to cause the signature-layer material to reach the heat front and emit at the early times observed in the experiments. For example, curve 3 ($\sigma_{rms} = 0.0304$ μm) in Fig. 8b yields signature times close to the observed burn-through time for the bare parylene target in Table I (-250 ps for 6 μm). If the initial mode spectrum were like that given by $\Delta R/R = 0.05$, larger initial values of σ_{rms} would be needed to produce the same signature time. The signature times from the mixing model should be used only as an indication because they were obtained with a simplified model of the evolution of the Rayleigh-Taylor instability and because they were based only on a reasonable guess of the amplitude and spectrum of the initial perturbations. The results do indicate, however, that for reasonable initial rms perturbation levels, the Rayleigh-Taylor instability could lead to the early mixing of low-Z ablator and signature materials.

The difference in the burn-through times between the bare parylene target and the Al-coated target can be explained as follows. Early shine-through can create density perturbations at the parylene–signature-layer interface in the form of a low density cavity, as was discussed previously. These perturbations can lead to larger Rayleigh-Taylor amplitudes than in the absence of shine-through because the initial rms amplitude levels are higher and because the Atwood number is larger (ρ_L is smaller). Fig. 8, which illustrates only the effect of increasing the rms of the initial perturbation, shows that the initial amplitude rms would have to be less than 0.03 μm to replicate the burn-through time for the targets with an aluminum barrier layer.

The effect of adding different types of barrier layers can be explained by the fact that the various layers let different amounts of laser light shine-through, producing variations in the initial perturbation. For example, KCl is probably more transparent to the laser light than aluminum, and thus the KCl-coated targets should sustain larger initial perturbations than the aluminum-coated target. Also, the difference in the burn-through time between the thick gold case and the thin gold case, which can be partially explained by the LILAC simulations from the increase in the amount of gold to be heated and ablated (about 60 ps out of the 225-ps difference), could be due to differences in the early shine-through (the thick gold layer is more opaque than the thin gold layer) and by increased radiation preheat from the thick gold barrier layer which radiates for a longer time than the thin one. Radiation preheat tends to decrease the density gradients in the target, thus reducing the Rayleigh-Taylor growth rate.

The preceding analysis of mixing due to the Rayleigh-Taylor instability may explain the fast burn-through rates observed in the experiment. However, it should be noted that, if the Rayleigh-Taylor instability were present, its effects on the overall implosion dynamics may not be observable experimentally. The thickness of the mixing region is less than 10

μm throughout the implosion (see Fig. 7), which is less than the resolution of the time-resolved imaging x-ray diagnostics (about 15 μm). Also, LILAC simulations of OMEGA gas filled and cryogenic target implosions[7] show reasonable agreement with experimental observables such as laser energy absorption, x-ray conversion for moderate Z materials, implosion velocity, and time of core formation. This indicates that the unperturbed one-dimensional flow obtained by LILAC approximates well the gross features of the implosions. Numerical simulations of the development of the nonlinear evolution of Rayleigh-Taylor unstable flow have shown that there exists no large departure in the motion of the centroid of mass of the shell between implosions that are uniform and those that are distorted due to unstable growth .[18] Therefore, if the Rayleigh-Taylor instability were present in the burn-through experiment, its presence could not be confirmed from the usual array of diagnostics deployed during OMEGA implosion experiments. It may be possible to do so with a framed x-ray backlighting system having a spatial resolution less than 2 μm (the typical size of the perturbations) and a temporal resolution below 10 ps to avoid blurring. Since this is currently beyond our diagnostic capabilities, we have planned further burn-through experiments to confirm indirectly the presence of the Rayleigh-Taylor instability. By using a signature layer with a mass density nearly equal to that of parylene we hope to greatly suppress the interface instability and be able to study the burn-though characteristics of targets in which the ablation surface instability should dominate.

CONCLUSIONS

Burn-through experiments have been carried out using targets coated with a barrier layer consisting of different materials and thicknesses. The results show that burn-through occurs progressively later during the pulse for the following succession of barrier layers:

none, aluminum, KCl, CsI, thin gold, and thick gold. Simulation results predict that there should be only small differences (~50 ps) between the burn-through time of all the barrier layers, except for the thick gold barrier layer. Several processes that could lead to fast burn-through rates have been considered: severe hot spots (intensities ten times nominal), shine-through, the presence of a prepulse, filamentation, self-focussing, and mixing due to the Rayleigh-Taylor instability. None of these processes, except mixing due to the Rayleigh-Taylor instability, could adequately explain the experimental results, either because measurements did not show their existence (severe hot spots, prepulse), because they were unaffected by the barrier layers (hot spots, self-focussing), or because 1-D simulations showed they had little effect (shine-through). We have shown that the Rayleigh-Taylor instability has the potential of mixing signature-layer material far enough into the parylene that early time x-ray emission from the signature layer would be observed. The effect of an opaque barrier layer is to prevent the target damage caused by shine-through, thus reducing the initial perturbations that seed the instability. Varying the material and the thickness of the barrier layer also affects the shine-through, thus affecting the magnitude of the seed of the instability. Since little is known about the transmission and breakdown characteristics of materials to 351-nm laser light at laser intensities below 10^{13} W/cm^2, experiments have begun that investigate the shine-through behavior of thin barrier layers.[27]

The experiments reported in this paper have shown that opaque barrier layers improve the behavior of parylene-coated targets when compared to one-dimensional simulations. Already, aluminum barrier layers are being used to improve the results of the high-density implosion experiments that are presently carried out on the OMEGA laser system. Finally, burn-through-type experiments with improved laser illumination uniformity could produce qualitative information on the mixing of the signature layer into

parylene due to the Rayleigh-Taylor instability. Such experimental results could be used to check the validity and the normalization of mixing models.

ACKNOWLEDGMENTS

The authors would like to thank Dr. R. Epstein for developing the non-LTE average-ion package in LILAC and for a thorough reading of the manuscript, Dr. R. Marjoribanks for useful discussions, the target fabrication group, and the members of the OMEGA laser and experimental operations groups. This work was supported by the U.S. Department of Energy Division of Inertial Fusion under agreement No. DE-FC03-85DP40200 and by the Laser Fusion Feasibility Project at the Laboratory for Laser Energetics which has the following sponsors: Empire State Electric Energy Research Corporation, New York State Energy Research and Development Authority, Ontario Hydro, and the University of Rochester. The research and materials incorporated in this work were partially developed at the National Laser Users Facility at the University of Rochester's Laboratory for Laser Energetics. Such support does not imply endorsement of the content by any of the above parties.

REFERENCES

1. LLE Review **23**, DOE/DP40200-03, 125 (1985).
2. J. Delettrez, R. Epstein, M. C. Richardson, P. A. Jaanimagi, and B. L. Henke, Phys. Rev. A **36**, 3926 (1987).
3. S. Skupsky and T. Kessler, Opt. Commun. **70**, 123 (1989).
4. B. L. Henke and P. A. Jaanimagi, Rev. Sci. Instrum. **54**, 1311 (1983).
5. P. A. Jaanimagi, L. DaSilva, G. G. Gregory, C. Hestdalen, C. D. Kiikka, R. Kotmel, and M. C. Richardson, Rev. Sci. Instr. **57**, 2189 (1986).
6. An earlier version of LILAC is described in Laboratory for Laser Energetics Report No. 16, 1976 (unpublished).
7. R. L. McCrory, J. M. Soures, C. P. Verdon, F. J. Marshall, S. A. Letzring, S. Skupsky, T. J. Kessler, R. L. Kremens, J. P. Knauer, H. Kim, J. Delettrez, R. L. Keck, and D.K. Bradley, Nature **335**, 225 (1988).
8. The extent of the smoothing of the hot spots from the superposition of the 24 beam of OMEGA cannot be easily estimated. While a point on the target is illuminated by 12 beams of OMEGA, only four beams contribute a significant amount of energy to the local intensity. The other beams contribute negligibly to the absorbed intensity because of their large angle of incidence. The smoothing factor is estimated to be between two and three, rather than four, because the contributing four beams impinge on the target at 41° to each other and are focused tangentially to the target surface.
9. A. Ng, D. Pasini, and P. Celliers, Appl. Phys. Lett. **44**, 713 (1984).

10. N. Bloembergen, IEEE J. Quantum Electron. **QE-10**, 375 (1974); LLE Review **35**, DOE/DP40200-74, 125 (1988); W. Seka (private communication).
11. H. Kim (private communication).
12. Spitzer and R. Härm, Phys. Rev. **89**, 977 (1953).
13. C. E. Max, Phys. Fluid **1**, 74 (1976); M. S. Shoda, A. K. Ghatak, and V. K.Tripath, Progress in Optics XIII, E. Wolf (Ed.), North-Holland (1976), p. 171.
14. W. L. Kruer, Comments Plasma Phys. Controlled Fusion **2**, 73 (1985).
15. LLE Review **28**, DOE/DP40200-26, 164 (1986).
16. G. J. Taylor, Proc. R. Soc. London, Ser. A **201**, 192 (1950); D. J. Lewis, Proc. R. Soc. London, Ser. A **202**, 81 (1950); S. Chandrasekhar, *Hydrodynamic and Hydromagnetic Stability*, (Clarendon Press, Oxford, England, 1961), Chap. 10.
17. H. Takabe, K. Mima, L. Montierth, and R. L. Morse, Phys. Fluid **28**, 3676 (1985).
18. M. H. Emery, J. H. Gardner, and J. P. Boris, Phys. Rev. Lett. **48**, 677 (1982).
19. C. P. Verdon. R. L. McCrory, R. L. Morse, G. R. Baker, D. I. Meiron, and S. A. Orszag, Phys. Fluid **25**, 1653 (1982).
20. K. I. Read, Physica **12d**, 45 (1984); D. L. Youngs, Physica **12d**, 32 (1984).
21. S. W. Haan, Phys. Rev. A **39**, 5812 (1989).
22. S. E. Bodner (private communication); M. Tabak (private communication).
23. ORCHID is a two-dimensional Lagrangian hydrodynamic code that is described in some length in Ref. 1

24. G. Birkhoff and D. Carter, J. Math. Mech. **6**, 769 (1957); P. R. Garabedian, Proc. R. Soc. London , Ser. A **241**, 423 (1957).

25. G. R. Baker, D. I. Meiron, and S. A. Orszag, Phys. Fluid **23**, 1485 (1980).

26. S. E. Bodner, J. Fusion Energy **1**, 221 (1981).

27. T. Boehly, D. K. Bradley, and J. Delettrez, Paper H6, 19th Annual Anomalous Absorption Conference, Durango, CO (1989); D. K. Bradley, T. Boehly, D. Brown, J. Delettrez, W. Seka, and D. Smith, *Laser Interaction and Related Plasma Phenomena* (to be published).

Figure Captions

Table I:

Onset times of the x-ray emission from the signature layer for the various barrier - layer targets. The measured burn-through times through 6 μm of parylene and the simulation burn-through times for increasing laser intensity are tabulated. All times are with respect to the peak of the pulse. The last column indicates the normalized intensity required in simulations to match the measured burn-through times.

Barrier Layer	Z	Laser Intensity (W/cm^2)	Burn-Through Times (ps)						
			Measured	Simulation					I_m/I_o
				1.5 I_o	2 I_o	3 I_o	5 I_o	10 I_o	
none	-	8.1×10^{14}	-250±20	~400	150	20	-100	-220	12.3±1.3
0.1-μm Al	13	7.5×10^{14}	-25±20	nb	~350(120)	70	-50	-170	4.1±0.4
0.1-μm KCl	18	8.2×10^{14}	-150±20	290	140	30	-80	-180	7.4±0.6
0.1-μm CsI	54	8.0×10^{14}	0±20	~400	160	40	-60	-160	4.1±0.2
0.015-μm Au	79	7.9×10^{14}	125±20	270	140	30	-60	-130	2.1±0.2
0.05-μm Au	79	7.9×10^{14}	350±20	320	210	160	-100	—	1.5

Time in parentheses is for the Al case run with the KCl laser conditions.

TC2608

Fig. 1:

Effect of a 0.1-μm Al barrier layer on the burn-through time for various thicknesses of parylene. The burn-through time is plotted as a function of the parylene areal density, which is equivalent to the parylene layer thickness in centimeters (the density of parylene is 1.1 g/cm^3). Each experimental point represents an individual target with a given parylene thickness. The simulation results bracket the nominal laser intensity range in the experiment.

Fig. 2:

Emission from the signature layer for various barrier-layer targets. The time is with respect to the peak of the laser pulse and the layer thickness in microns. The parylene continuum emission has been subtracted.

Fig. 3:

Dependence of the burn-through time on the normalized laser intensity for targets without a barrier layer (bare) and with an Al and KCl barrier layer. The horizontal bands are the experimental times from Fig.2. The width of the bands is the experimental uncertainty.

Fig. 4:

Calculated density profiles in the corona 300 ps before the peak of the pulse for four targets at nominal intensity: bare , 0.1 μm of Al, 0.015 μm of Au, and 0.05 μm of Au barrier layers. The thicker part of the profile shows where the barrier-layer material is present. At this time, the nominal laser intensity is 4.7x10^{14} W/cm^2 and the laser intensity

at 0.1 critical is 2.0×10^{14} W/cm^2. The initial target radius was 150 μm. The density profile of the 0.05-μm Au case is shifted to the left for clarity.

Fig. 5:

Temporal evolution of the distance between the 0.1-critical-density surface and the critical density surface for the four targets described in Fig. 4. Time is with respect to the peak of the pulse. The measured burn-through time for the bare-parylene target is indicated as a reference.

Fig. 6:

ℓ-mode spectral distribution of the initial perturbation for the two values of $\Delta R/R$ used in estimating the mixing region thicknesses. The vertical axis is the rms amplitude over the azimuthal (m) modes. The perturbations are assumed to be symmetric in the azimuthal direction.

Fig. 7:

Results of the Rayleigh-Taylor instability mixing model for a 3-μm glass shell coated with (a) 4 μm of parylene and (b) 6 μm of parylene. The solid line is the temporal evolution of the parylene thickness and the dashed lines the evolution of the thickness of the unstable (mixing) region for the ablation surface instability (A) and the glass-parylene interface instability (I). The initial perturbation has a $\sigma_{rms} = 0.167$ μm and $\Delta R/R = 0.05$ in both cases. The earliest crossing of the solid line and a dashed line is taken as the onset time of emission from the glass shell due to mixing.

Fig. 8:

Onset time of emission from the glass shell obtained from the mixing model as a function of the parylene thickness for $\Delta R/R = 0.05$ (a) and 0.01 (b). Curves 1, 2, and 3 are for initial perturbations with $\sigma_{rms} = 0.304$ μm, 0.167 μm, and 0.0341 μm, respectively. The solid rectangle of the end of curve 3 for $\Delta R/R = 0.05$ indicates the signature layer does not mix through the parylene layer for larger thicknesses.

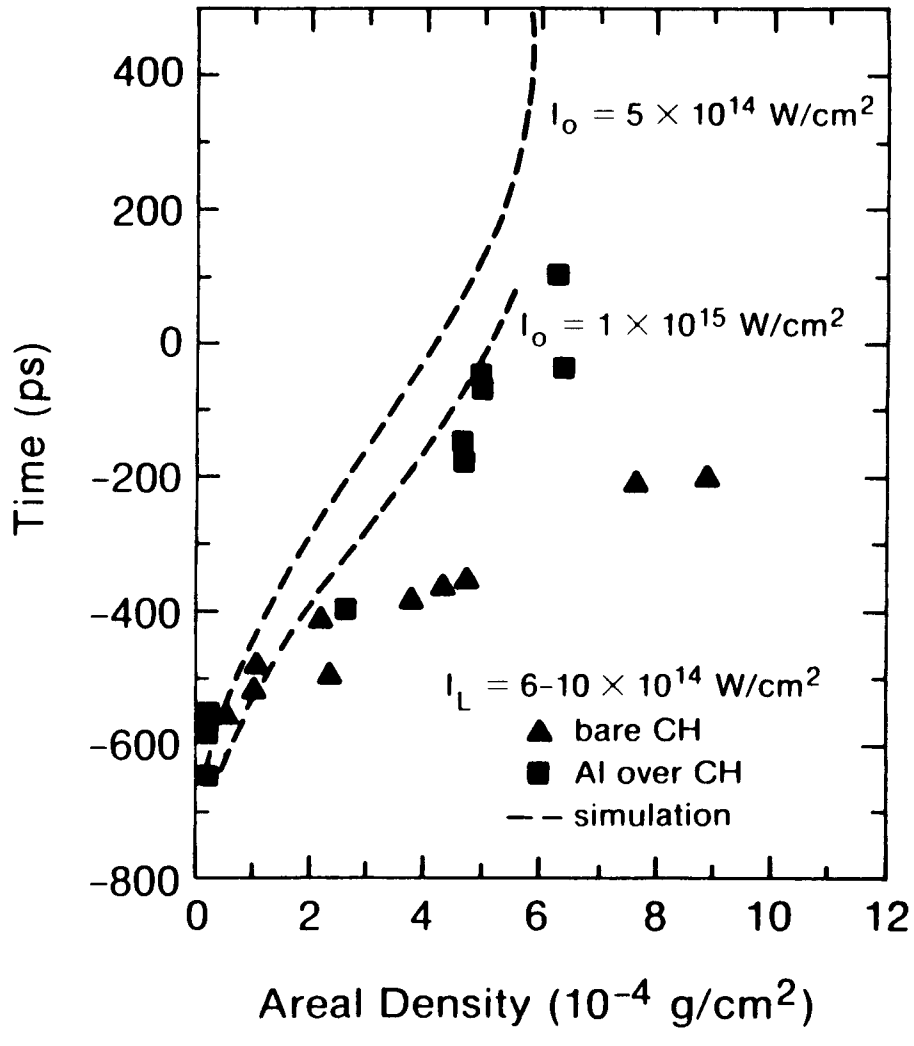
400
200
0
-200
-400
-600
-800
Time (ps)
0
2
4
6
8
10
12
Areal Density (10^{-4} g/cm^2)
$I_o = 5 \times 10^{14}$ W/cm^2
$I_o = 1 \times 10^{15}$ W/cm^2
$I_L = 6\text{-}10 \times 10^{14}$ W/cm^2
bare CH
Al over CH
simulation

TC2604

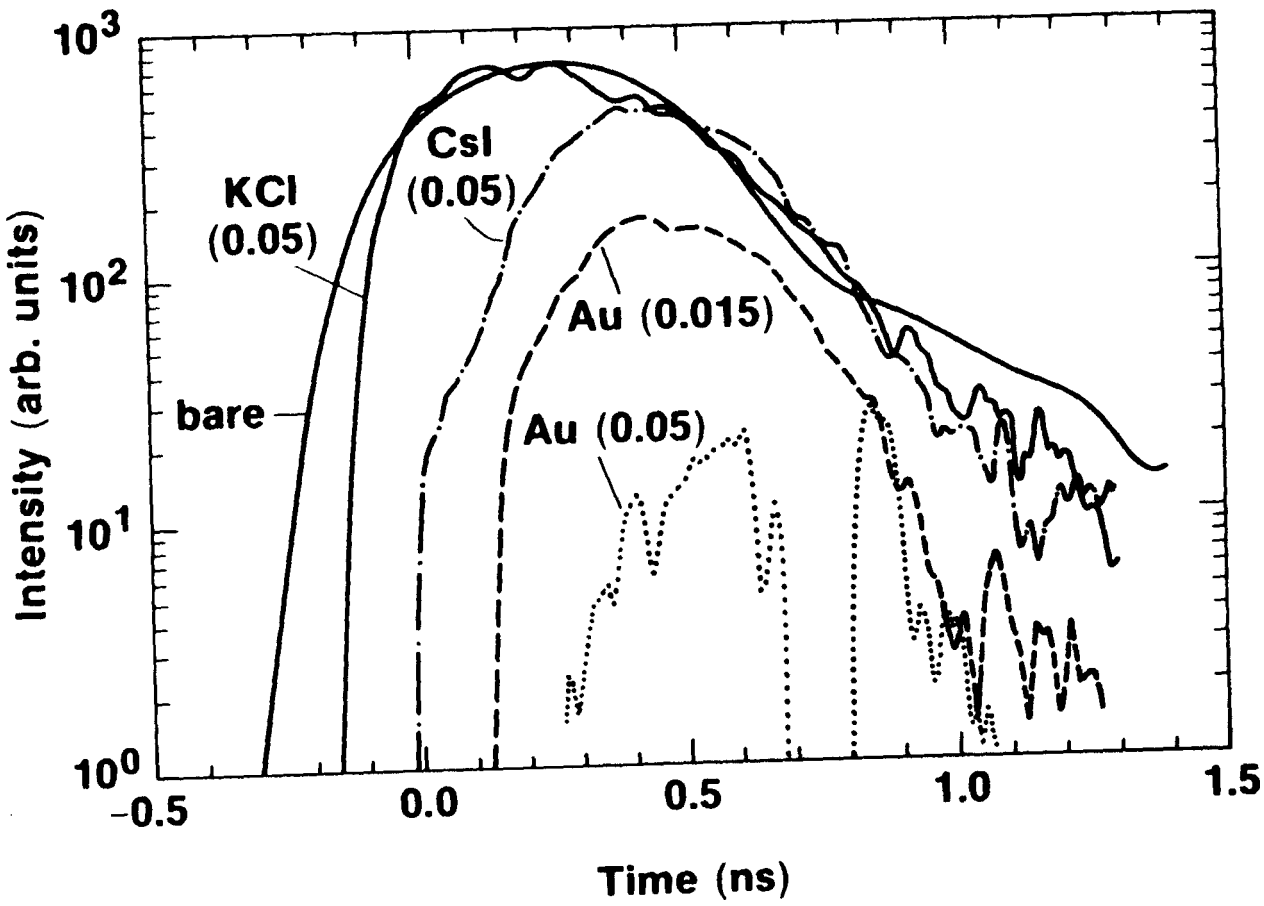
10^3
10^2
10^1
10^0
Intensity (arb. units)
KCl
(0.05)
CsI
(0.05)
Au (0.015)
bare
Au (0.05)
-0.5
0.0
0.5
1.0
1.5
Time (ns)

E4645

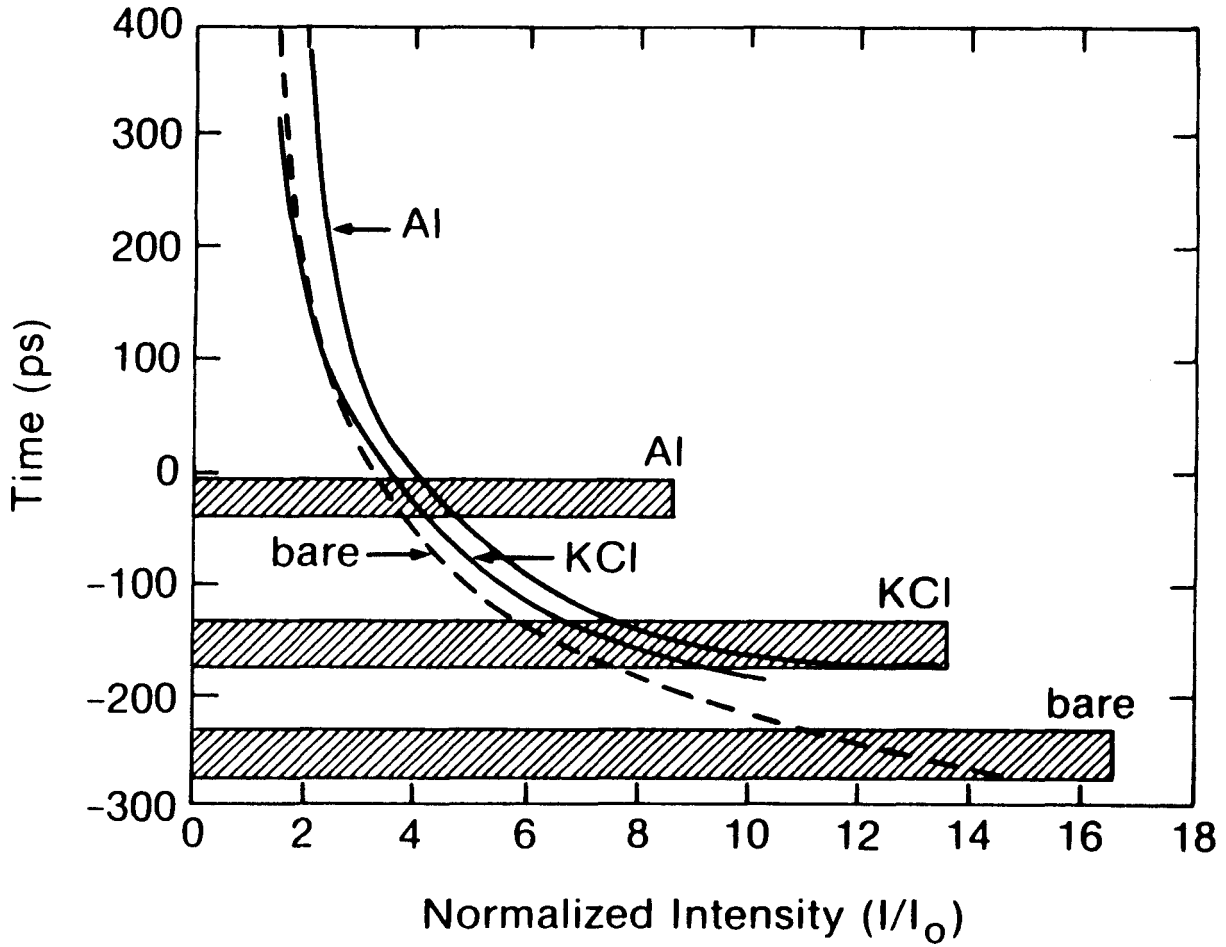
400
300
200
100
0
-100
-200
-300
Time (ps)
Al
Al
bare
KCl
KCl
bare
0
2
4
6
8
10
12
14
16
18
Normalized Intensity (I/I$_o$)

TC2605

$I_L = 4.7 \times 10^{14}$ W/cm^2

I (at 0.1 n_c) $= 2.0 \times 10^{14}$ W/cm^2

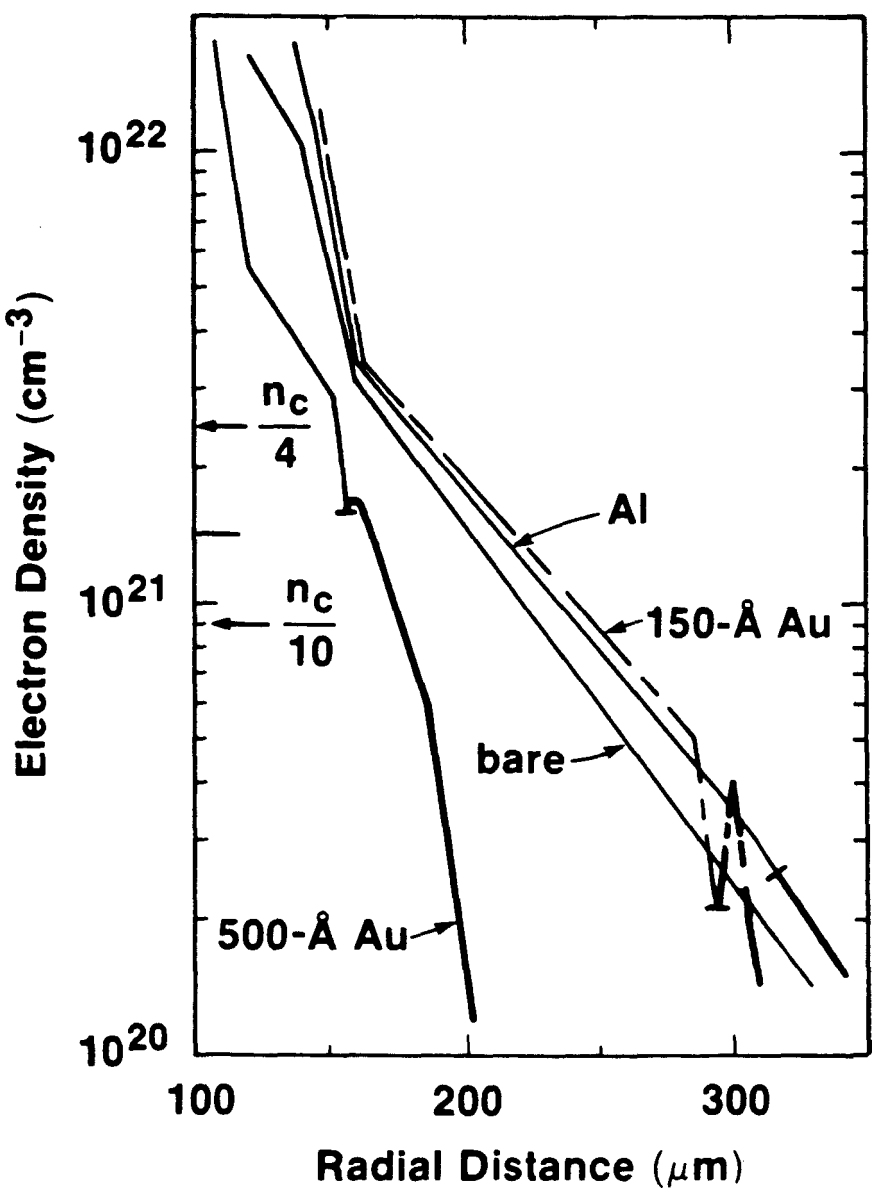

TC2377

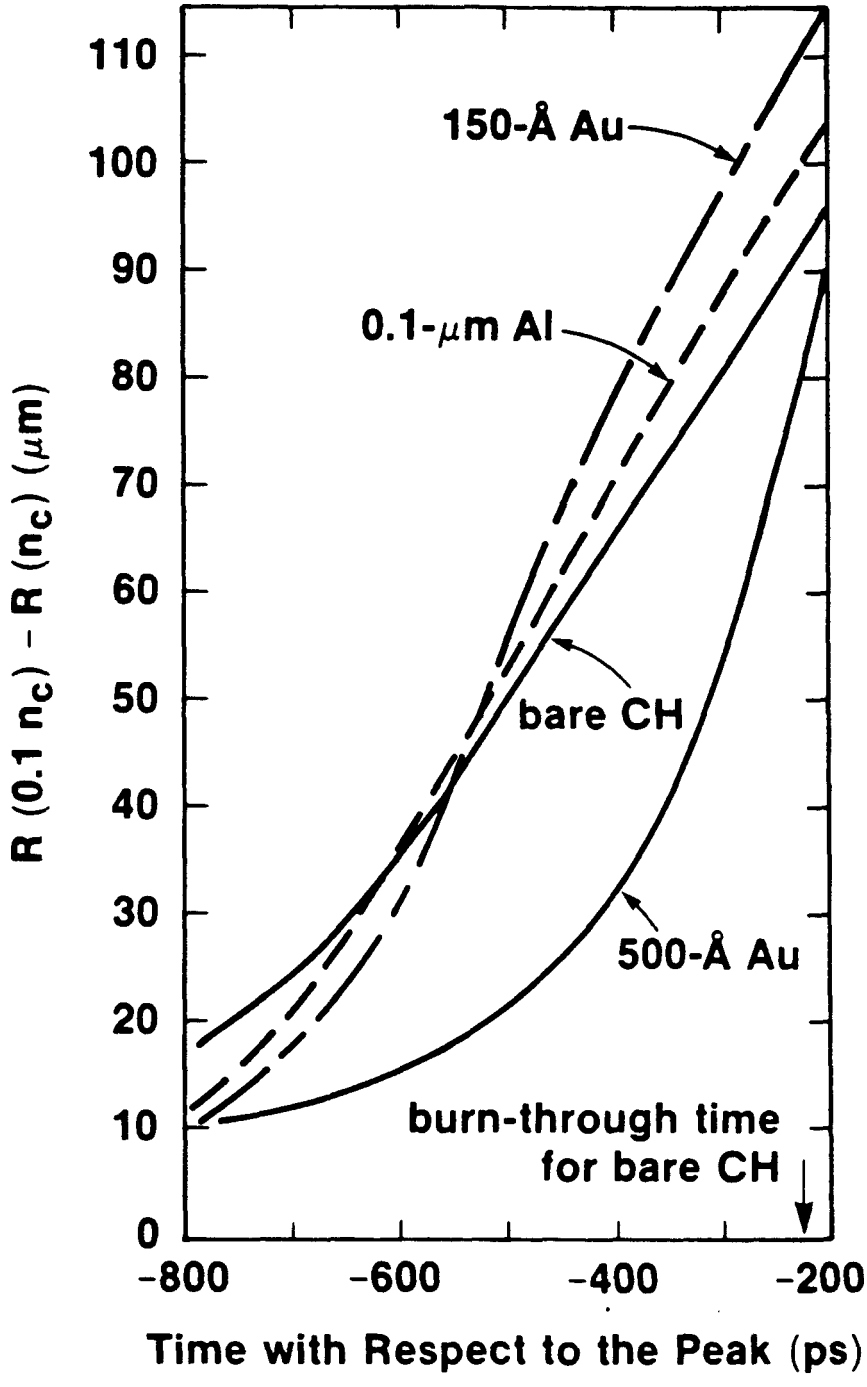
110
100
90
80
70
60
50
40
30
20
10
0
150-Å Au
0.1-μm Al
bare CH
500-Å Au
burn-through time
for bare CH
-800
-600
-400
-200
R (0.1 nc) - R (nc) (μm)
Time with Respect to the Peak (ps)

TC2375

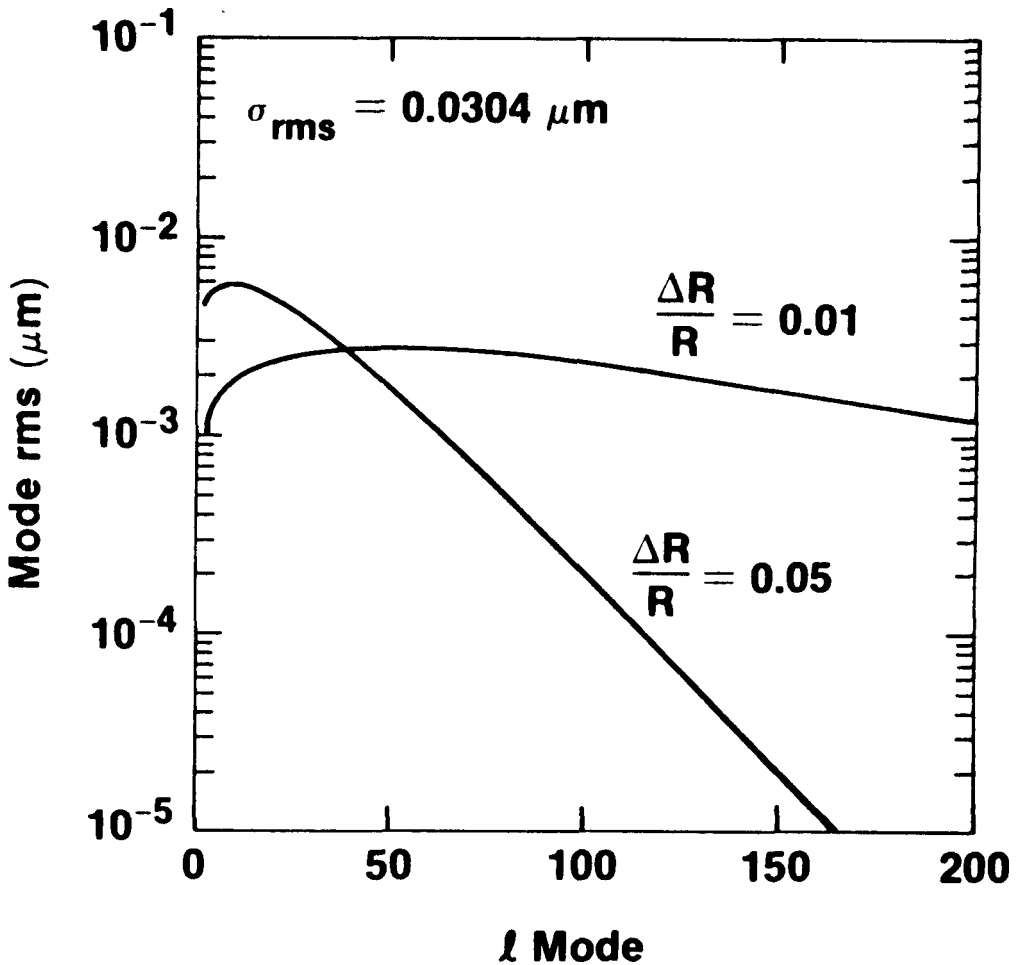
10^{-1}
10^{-2}
10^{-3}
10^{-4}
10^{-5}
$\sigma_{rms} = 0.0304\ \mu m$
$\frac{\Delta R}{R} = 0.01$
$\frac{\Delta R}{R} = 0.05$
Mode rms (μm)
0
50
100
150
200
ℓ Mode

TC2741

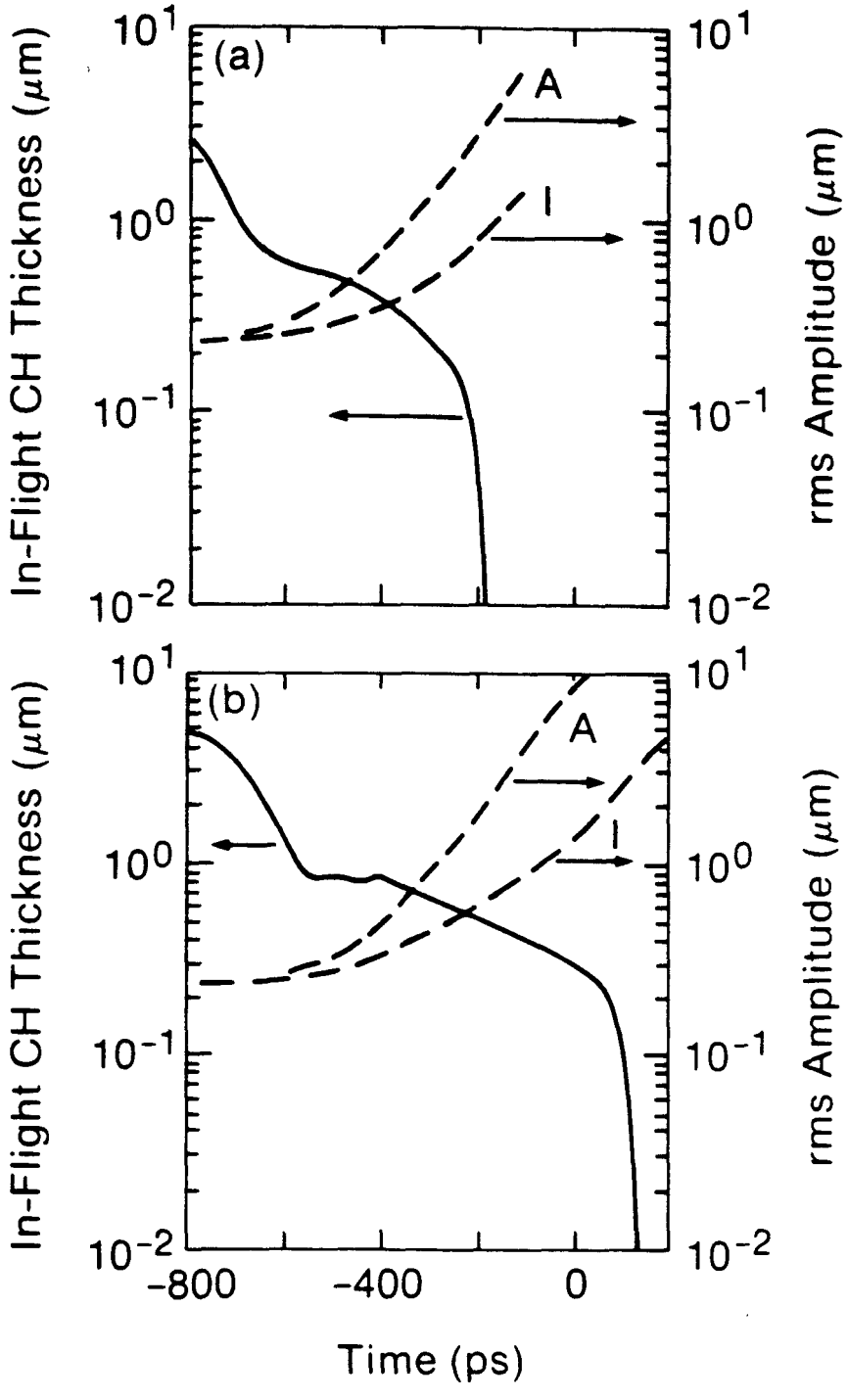
(a)
(b)
A
I
In-Flight CH Thickness (μm)
rms Amplitude (μm)
10^1
10^0
10^{-1}
10^{-2}
-800
-400
0
Time (ps)

TC2606

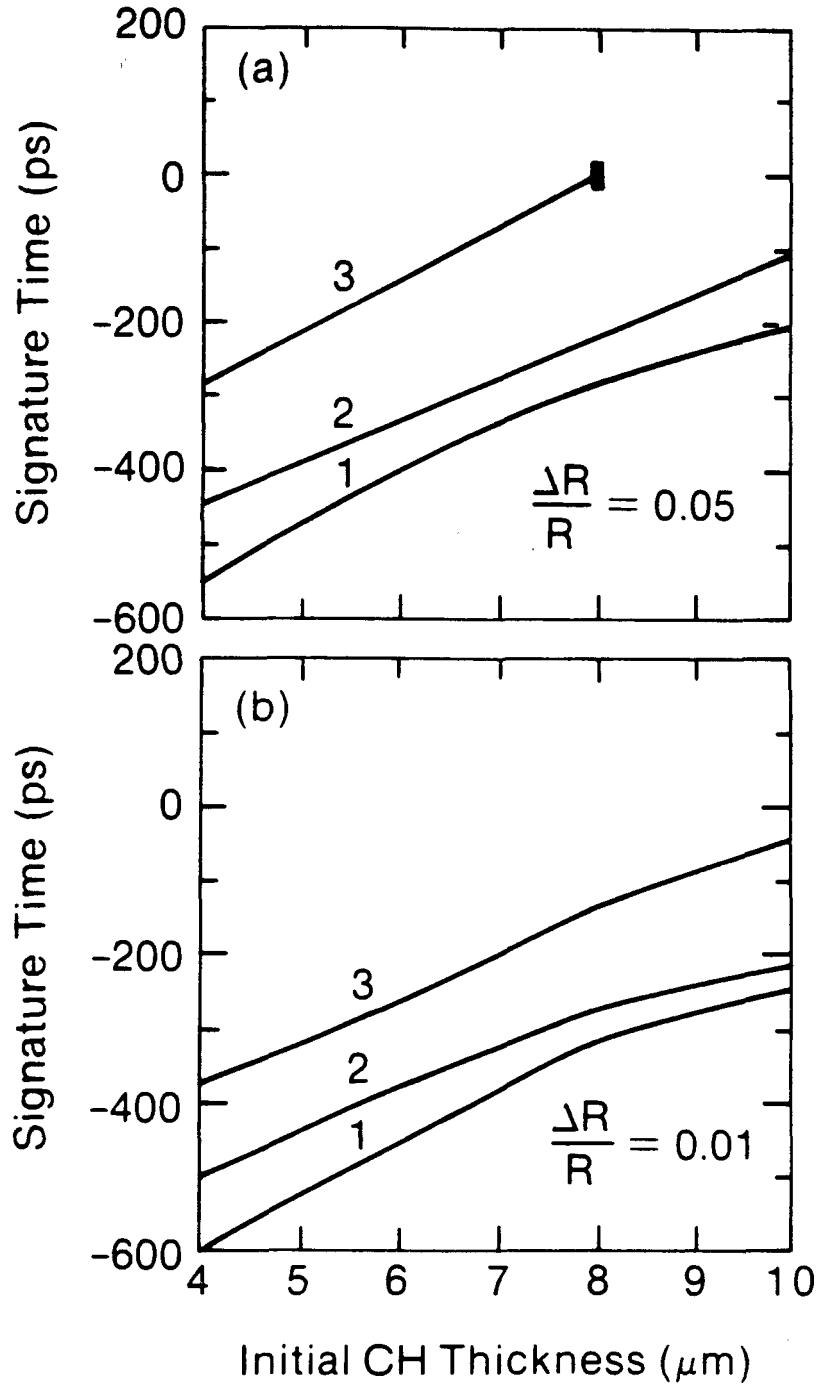
200
0
-200
-400
-600
(a)
Signature Time (ps)
3
2
1
ΔR/R = 0.05
200
0
-200
-400
-600
(b)
Signature Time (ps)
3
2
1
ΔR/R = 0.01
4
5
6
7
8
9
10
Initial CH Thickness (μm)

TC2607